ADVANCES IN FOREST FIRE RESEARCH

2022

Edited by
**DOMINGOS XAVIER VIEGAS
LUÍS MÁRIO RIBEIRO**

The role of helicity and fire-atmosphere turbulent energy transfer on potential wildfire behavior

Jiawei Zhang*[1;2]; Marwan Katurji[2]; Peyman Zawar-Reza[2]; Tara Strand[1]

[1] *New Zealand Forest Research Institute, Scion, New Zealand, {jiawei.zhang@scionresearch.com}*
[2] *School of Earth and Environment, University of Canterbury, New Zealand,*

*Corresponding author

Keywords

Fire-atmosphere interaction, Turbulence, Energy transport, Large eddy simulation

Abstract

Understanding near surface fire-atmosphere interactions at turbulence scale is fundamental for predicting fire spread behavior. This study investigated the fire-atmosphere interaction and the accompanying energy transport processes within the convective boundary layer. Three groups of large eddy simulations (LES) representing common ranges of convective boundary layer conditions (resulting from land surface heat flux ranging from 120 to 360W/m2) and fire intensities (50 to 150kW/m2) were used to examine how ambient buoyancy-induced atmospheric turbulence can impact fire region heat and momentum transport.

In a relatively weak convective boundary layer, the change of near-surface atmospheric turbulence caused by the buoyancy force from the fire heat release is substantial and can cause an anticorrelation of the helicity between the ambient atmosphere and the fire-induced flow. Fire-induced impact becomes much smaller in a relatively strong convective environment with ambient atmospheric flow maintaining coherent structures including vortices across the fire heating region. The helicity also shows strong correlation between the ambient atmosphere and the fire-induced flow. A further energy transport efficiency analysis shows a narrow heat transport zone above the fire line for the weak convective boundary layer scenario. This indicates confined heat release and stronger fire-induced buoyancy force. The high-efficiency heat transport zone becomes much wider in a stronger convective boundary layer which leads to a wider distribution of heat released from fire, the weaker fire-induced buoyancy force and causes less fire-induced flow-field change. The work also found counter-gradient transport zones of both momentum and heat in fire cases in the weak convective boundary layer group. The counter-gradient transport might indicate the existence of strong buoyancy-induced mixing processes.

1. Introduction

Atmospheric motions vary in scale from thousands of kilometers (planetary circulations) to sub-meter turbulence eddies (Orlanski, 1975). These atmospheric motions can interact and influence fire behavior at different scales and aspects (Potter, 2002). The thermal internal boundary layer caused by localized heating of fire, and the atmospheric boundary layer (ABL) that envelops it, develop at integral time scales spanning from seconds to tens of minutes (Stull, 2012). Within this fire turbulence environment (hereafter referred to as the FTE, Figure 1), atmospheric turbulence plays an important part in energy transfer between the fire and the surrounding atmosphere ((Dickinson et al., 2021; Finney et al., 2015; Kremens et al., 2012; Sullivan, 2017).

Quantifying turbulent heat and momentum fluxes is important to better describe the coupled processes within the FTE which can lead to spatial and temporal variation in fire behavior. This work aims to describe the role of the background atmospheric flow in fire-atmosphere interactions and discuss the physical mechanisms driving these interactions. The main objective is to understand processes that control the spatial and temporal development of turbulent heat and momentum transport under different convective boundary layer (CBL) turbulence intensities.
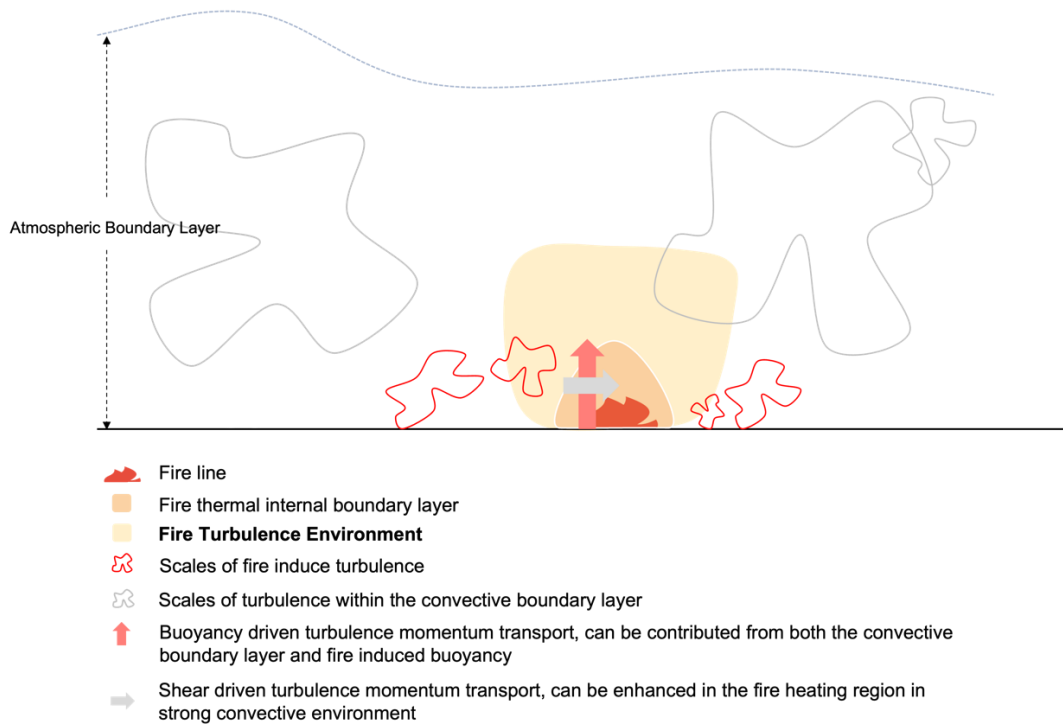
Atmospheric Boundary Layer

- Fire line
- Fire thermal internal boundary layer
- **Fire Turbulence Environment**
- Scales of fire induce turbulence
- Scales of turbulence within the convective boundary layer
- Buoyancy driven turbulence momentum transport, can be contributed from both the convective boundary layer and fire induced buoyancy
- Shear driven turbulence momentum transport, can be enhanced in the fire heating region in strong convective environment

Figure 1- Conceptual diagram showing the fire turbulence environment (FTE).

The impact of different fire intensities for each turbulence regime is also considered using a 2D hot patch with different fixed heat flux intensities. The novel quantitative partitioning of heat and momentum flux using spatially distributed energy partitioning (referred to as spatial quadrant analysis) allowed the definition of spatial energy transfer zones that define the scales and intensities of these interactions. Finally, and by calculating the helicity above the fire region influenced by atmospheric motion, the potential for fire behavior influenced by atmospheric turbulence is discussed in relation to fire and atmospheric turbulence intensity levels.

2. Methods

2.1. Model description and set-up

The PArallelized LES Model (PALM) model (Maronga et al., 2015; Raasch & Schröter, 2001) is the model employed here . A matrix of simulations was carried out with three ambient land surface heat fluxes and three fire intensities (Table 1). A base case, with no simulated fire, was also run for every ambient land surface heat flux group to represent the ambient atmospheric flow field. In all cases, three nested domains with one-way nesting were used, downscaling from 32m to 4m grid resolution (Figure 2). A 12m wide 2D hot patch with different heat fluxes was placed in the center of the inner-most domain (D3) to represent fire with different intensities for the fire cases.

Table 1- Simulation naming convention including a total of 12 simulations. Note the difference in magnitude between the land surface heat flux and the fire intensities.

Group	Land Surface Heat Flux	Fire Intensity			
		Base	Low	Med	High
C1	$120\ W\ m^{-2}$				
C2	$240\ W\ m^{-2}$	No Fire	$50\ kW\ m^{-2}$	$100\ kW\ m^{-2}$	$150\ kW\ m^{-2}$
C3	$360\ W\ m^{-2}$				

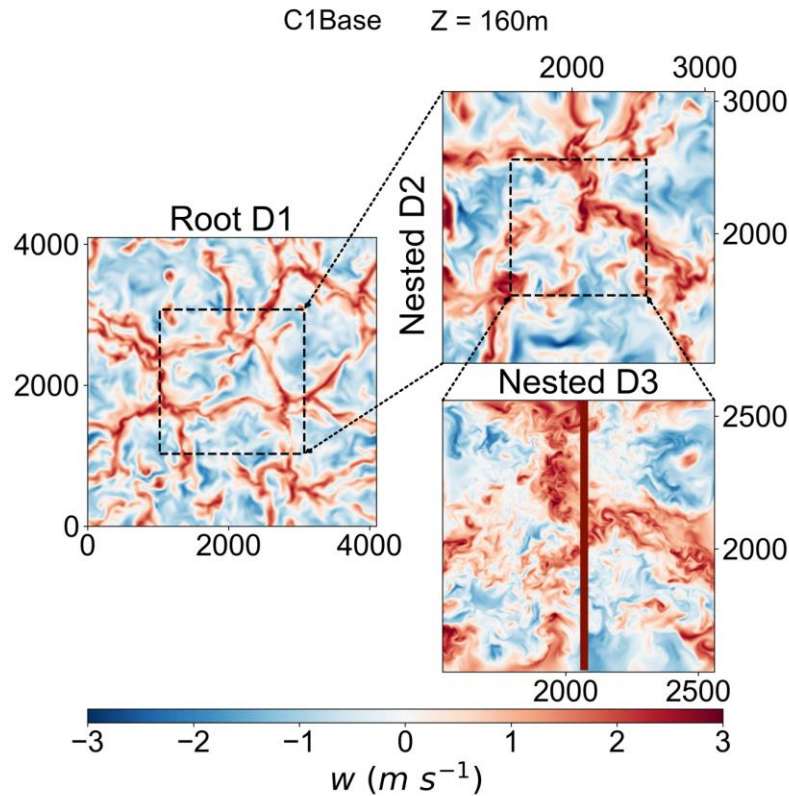***Figure 2. Instantaneous horizontal cross-section of vertical velocity at 160m above ground level (AGL) (z=160m) from one of the simulations (C1Base). D1, D2, D3 are for the nested Domains 1 (root or outermost domain), 2 and 3 (innermost domain). The red line in the D3 domain illustrates the hot patch location which was only set up at the surface of the fire cases after 03:30:00 simulation time.***

The same initial profiles were used for all the simulations. For the potential temperature profile, constant potential temperature of 293K is used from the surface up to 1km with an inversion then applied. The initial wind speed is set to be 0m/s at all locations. All cases were run for 4 hours with the first 3 hours as spin up period and the fire set up after 3.5 hours.

2.2. Helicity

Helicity is used to explore the changes or transfer of vorticity caused by the interaction between the fire-induced buoyancy and the ambient atmospheric flow. The helicity is calculated using the non-integral form (Equation 1). To better quantify the domain-wide helicity, the averaged magnitude of the vertical helicity component is calculated from the horizontal cross-section of the innermost (D3) domain.

$$H = (\nabla \times \vec{v}) \cdot \vec{v} \quad (1)$$

where $\vec{v}$ is the velocity vector and $\nabla \times \vec{v}$ is the vorticity vector $\vec{\omega}$.

2.3. Quadrant analysis

In any point location, the time series of instantaneous vertical transfer of horizontal momentum (w'u') and kinematic heat flux (w'θ') can be drawn in the Cartesian coordinate system with w' and the respective perturbation variable as the coordinates (Figure 3; Shaw et al., 1983). Each quadrant in the coordinate system has different physical interpretation.
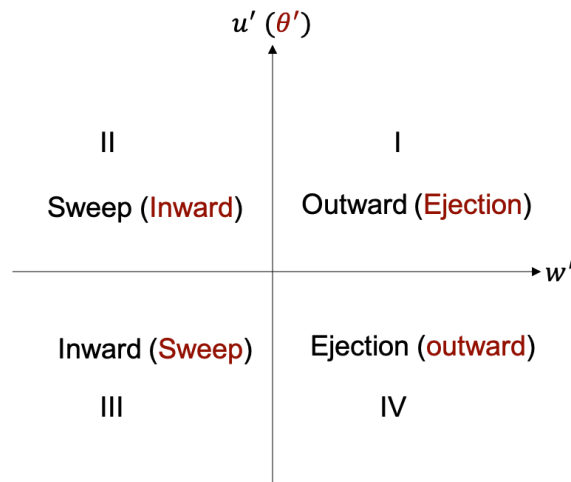
$u'\ (\theta')$

II

Sweep (Inward)

I

Outward (Ejection)

w'

Inward (Sweep)

Ejection (outward)

III

IV

Figure 3. The terminology and convention used for the quadrant analysis. A time series of w'u' (or w'θ') can be classified into each quadrant. For the momentum flux (w'u'), quadrants I and III represent the outward and inward motions which account for counter-gradient momentum transport. Quadrants II and IV represent the sweep and ejection motions and contribute to downgradient momentum transport. For the instantaneous kinematic heat flux (w'θ'), the sweep/ejection and outward/inward quadrants are reversed and illustrated using the red color.

Based on quadrant analysis, Wyngaard and Moeng (1992) implemented the concept of energy transport efficiency, which was defined as the ratio of downgradient flux to total flux. The mathematical form of energy transport efficiency is further discussed by Li and Bou-Zeid (2011) and is shown below,

$$\eta = \frac{F_{\text{total}}}{F_{\text{downgradient}}} = \frac{\overline{w'c'}}{\overline{w'c'}_{\text{ejections}} + \overline{w'c'}_{\text{sweeps}}} \tag{2}$$

where c represents variables like velocity, temperature or other scalars. The flux in each quadrant is calculated using the equation below,

$$\overline{w'c'}_i = \frac{1}{t} \sum_{j=t_0}^{t} w_j'\, c_j'\, I_{ij} \tag{3}$$

where I_j is defined as,

$$I_{ij} = \begin{cases} 1 & \text{if } w_j'c_j' \text{ is in quadrant } i \\ 0 & \text{otherwise} \end{cases} \tag{4}$$

From the above definition, the transport efficiency (η) is positive when the F_{total} and $F_{downgradient}$ have the same sign. This means the down-gradient transport is dominating the energy transport process and the turbulence is mainly shear driven. On the other hand, when the counter-gradient transport component is strong enough to counteract the down-gradient transport, the transport efficiency can be very small and even negative. To obtain spatial information about the momentum and heat transport within the FTE, the work extended the transport efficiency to the spatial modelling data.

3. Results

3.1. General flow patterns

Figure 4 shows the horizontal cross-section of the 1-minute averaged u velocity component at 10m above ground level (AGL) after the fire had been set up for 20 minutes. In the C1 group, a clear fire-induced convergence zone is formed across all fire cases while no such zone exists in the base case. In the C2 group, vortex structures can be found in both the ambient atmosphere (represented by the base case) and the fire cases. These vortex structures remain and are strengthened with the addition of the simulated fire. All C3 group cases show similar flow patterns with predominant negative values in the center of the domain and positive values at the edge.

Although not shown here, the fire cases in the C2 and C3 group maintain similar flow patterns of all velocity components to the respective base case up until 20 minutes after the fire line set-up.
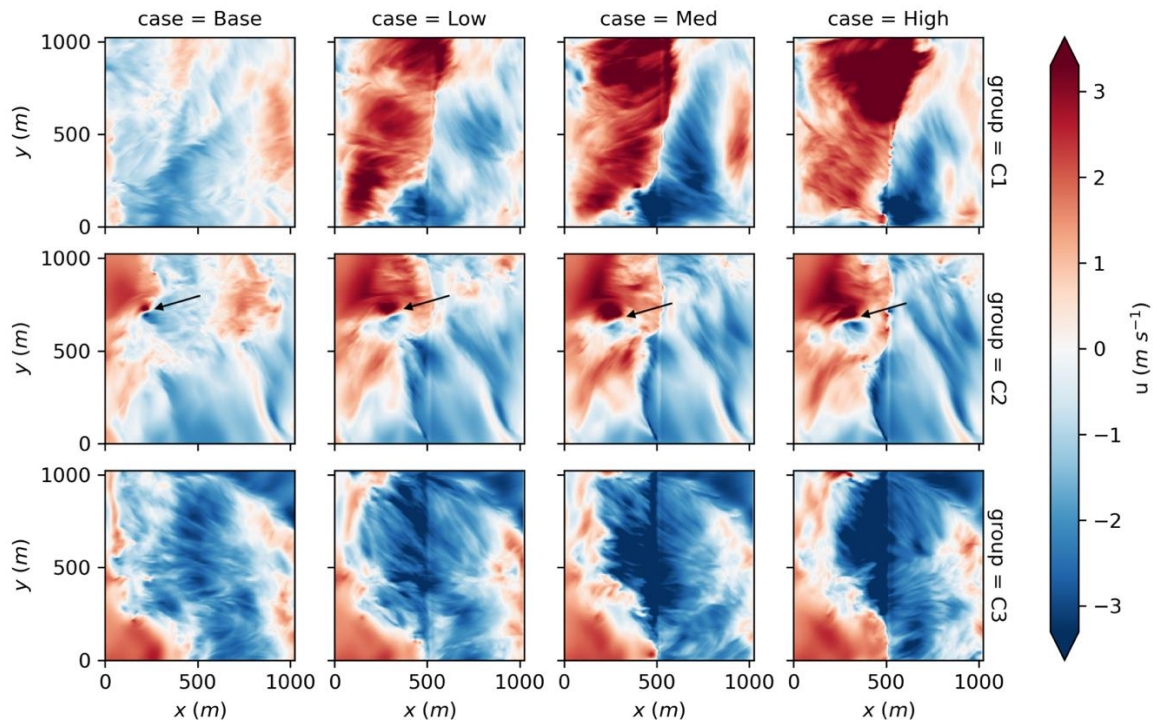

Figure 4. Horizontal cross-section (10m AGL) of 1-minute averaged horizontal u-velocity component 20 minutes after the fire lines were set up). Each row represents simulation groups with different ambient land surface heat flux (120W/m² for the C1 group, 240W/m² for the C2 group and 360W/m² for the C3 group). From left to right, each column represents the fire line intensity (heat flux) (no fire for the base case, 50kW/m² for the low intensity fire scenario, 100kW/m² for the medium intensity scenario and 150kW/m² for the high intensity scenario).

The temperature anomaly caused by fire also shows distinctive characteristics between C1 and the two other groups. Even 10 minutes after the fire line is set up, the high temperature zone caused by the fire maintains a relatively straight and narrow line at 10m AGL in all fire cases in the C1 group (Figure 5). Conversely, the high temperature anomaly in the fire cases in the C2 and C3 groups show much wider horizontal extent. From the vertical cross-section (not shown here), this is caused by tilting of the hot plume.
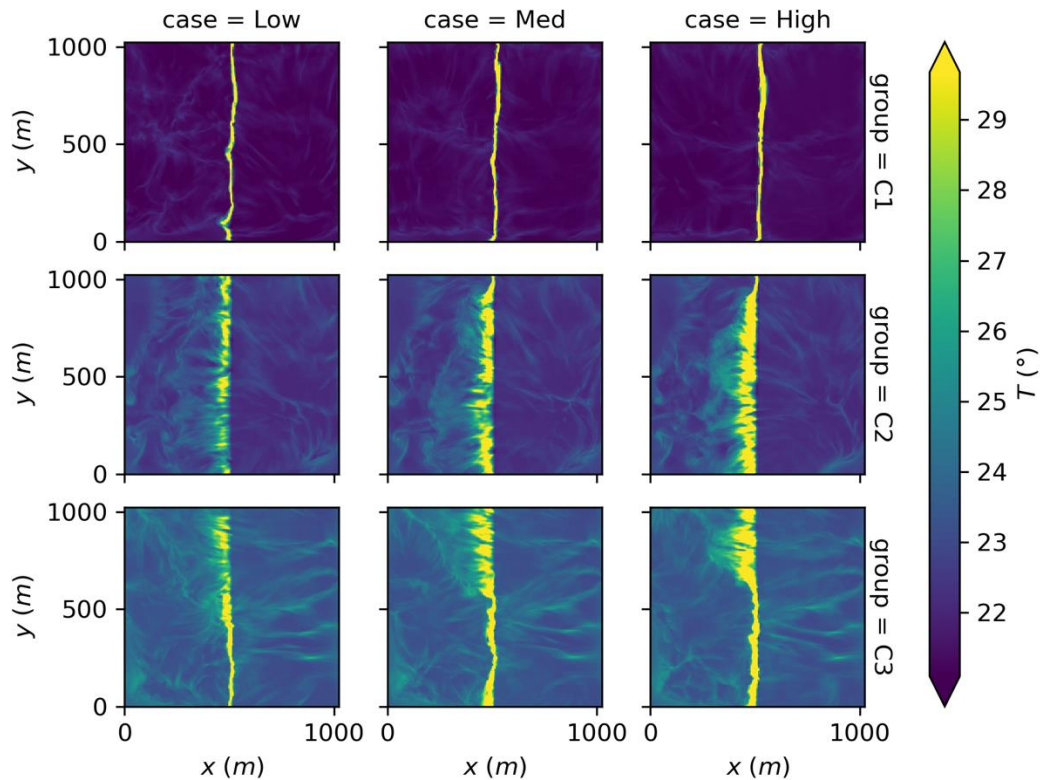
Figure 5. Horizontal cross-section (10m AGL) of 1-minute averaged air temperature after 20 minutes of the fire lines being set up). Each row represents simulation groups with different ambient land surface heat flux (120W/m² for the C1 group, 240W/m² for the C2 group and 360W/m² for the C3 group). From left to right, each column represents the fire line intensity (heat flux) (50kW/m² for the low intensity fire scenario, 100kW/m² for the medium intensity scenario and 150kW/m² for the high intensity scenario).

3.2. Helicity

The magnitude of the domain average vertical helicity component ($|H_z|$) is much lower in the base case in the C1 group (Table 2a) while the magnitude is higher in the base cases in the C2 and C3 groups. In all groups, fire cases have higher $|H_z|$ which might be caused by the reorganizing and tilting of the ambient vortices from the fire-induced buoyancy. This aligns with the framework suggested by Potter et al. (2012).

Table 2a- Average magnitude of the vertical helicity component $|H_z|$ at 10m AGL.

$|H_z|$	Base	Low	Med	High
C1 group	0.009	0.018	0.026	0.030
C2 group	0.015	0.023	0.028	0.031
C3 group	0.019	0.026	0.030	0.033

Table 2b- Correlation coefficient (r) of the vertical helicity magnitude $|H_z|$ time series (domain averaged at 10m height) between fire cases and the base (no fire) case from the same group.

r	Base	Low	Med	High
C1 group	N/A	-0.74	-0.76	-0.77
C2 group	N/A	0.69	0.55	0.60
C3 group	N/A	0.86	0.90	0.87

Time series of $|H_z|$ show some similarity between the fire cases and the base case, especially in the C2 and C3 groups (Figure 6). The similarity can be confirmed by the correlation coefficient (Table 2b). In general, fire cases and the ambient atmospheric flow represented by respective base cases have high correlation coefficients up to 0.9 in the C2 and C3 groups. The high correlation coefficients indicate that ambient atmospheric flow can maintain its coherent turbulent flow structures and impact fire behaviors under the convective boundary layer conditions similar to the C2 and C3 groups. On the other hand, strong anticorrelation can be found between the fire cases and the base case in the C1 group which means an increase of $|H_z|$ in the fire cases corresponds to a decrease of the $|H_z|$ in the ambient atmosphere. This indicates that fire-induced processes like vortex stretching/tilting might be dominating and changing the rotational flow field in a relatively weak convective boundary layer.
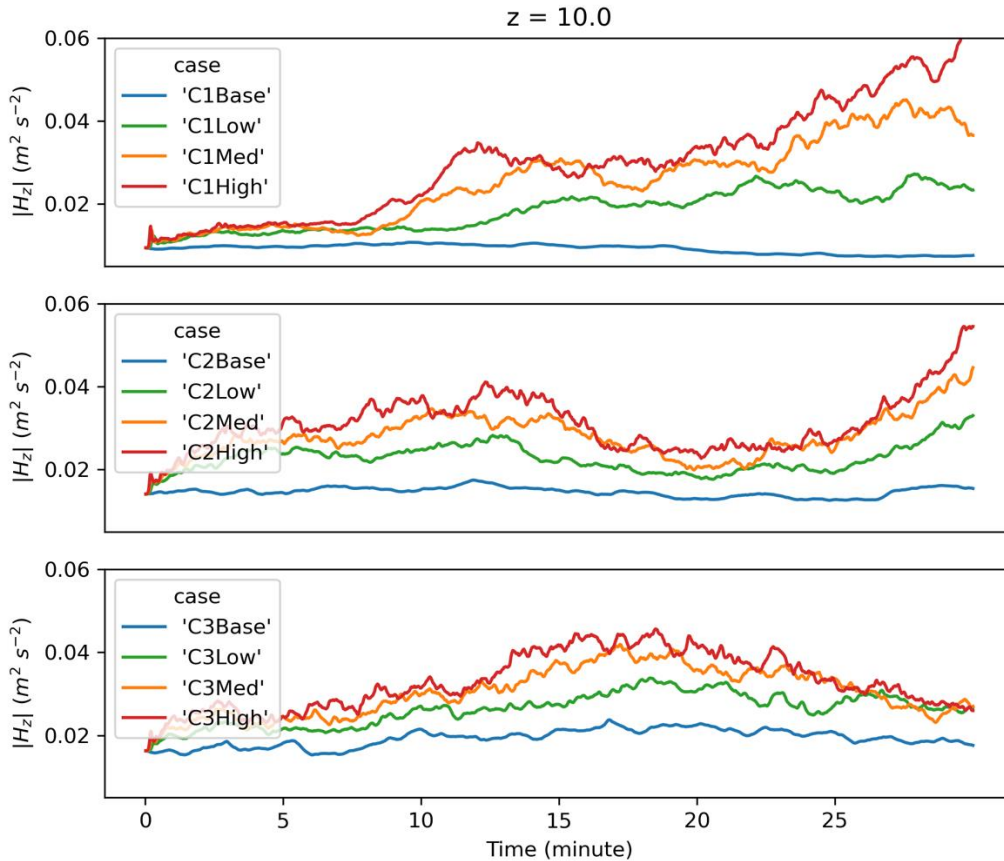
Figure 6. Time series of the vertical helicity magnitude (domain averaged at 10m AGL) from each case in each simulation group from the moment fire was set up. (a), (b), (c) show results in the C1, C2 and C3 groups respectively while blue, green, orange, and red lines represent base (no fire), low, medium, and high intensity fire case in each group respectively.

3.3. Energy transport efficiency

While the above analysis has shown evidence of different fire-atmosphere interaction under different CBL conditions, to understand the physical processes behind these results, the turbulent transport efficiency is further investigated.

Horizontal and vertical cross-sections of the vertical heat transport efficiency ($\eta_{w'\theta'}$) from all cases are shown in Figures 7 and 8. From both horizontal and vertical cross-sections, a much narrower and more distinctive high-efficiency transport zone can be found in the C1 group compared to other groups. In both the C1 and C2 groups, counter-gradient heat transport zone (negative values) can be found.
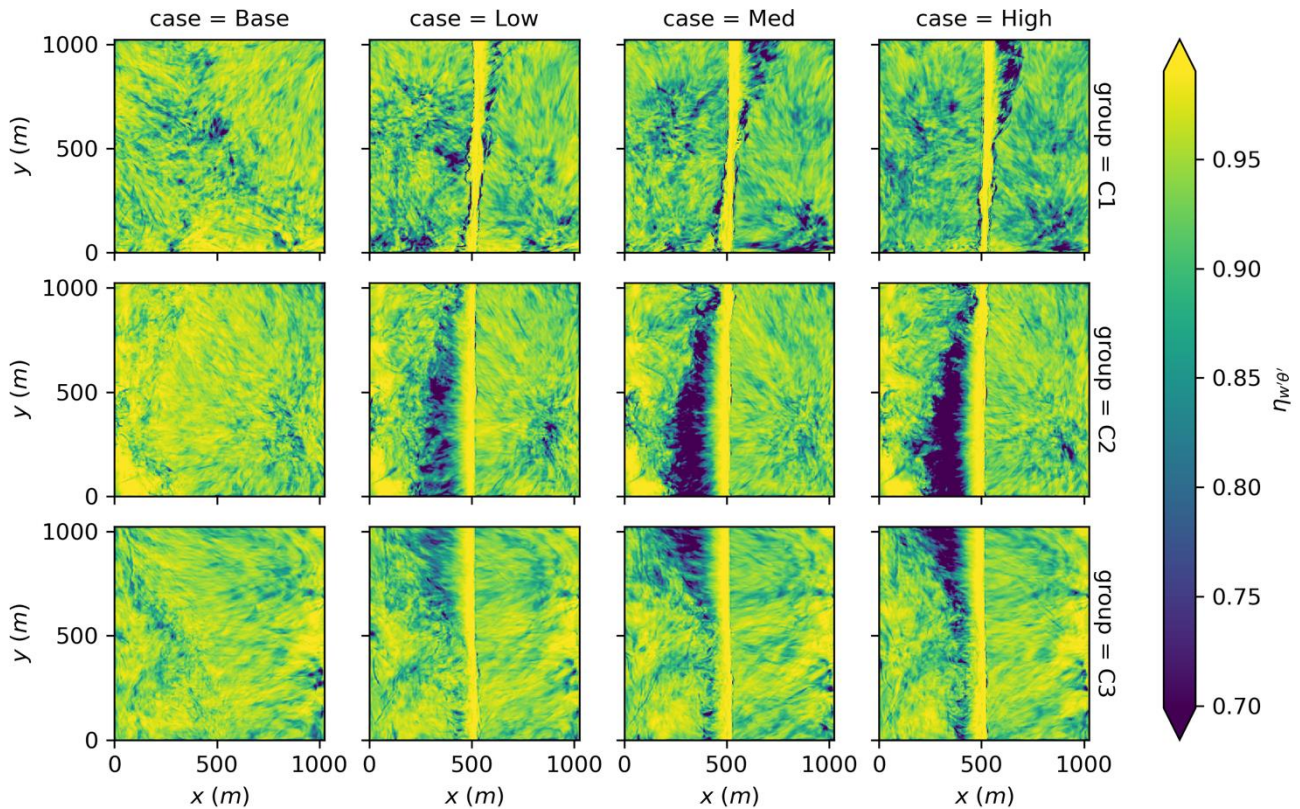
Figure 7. Horizontal cross-section of heat transport efficiency η_{w′θ′} at 10m above the surface from all cases during the first 15 minutes of the fire being set up. Each row represents different groups while each column represents either the base cases or the cases with the different fire intensities.
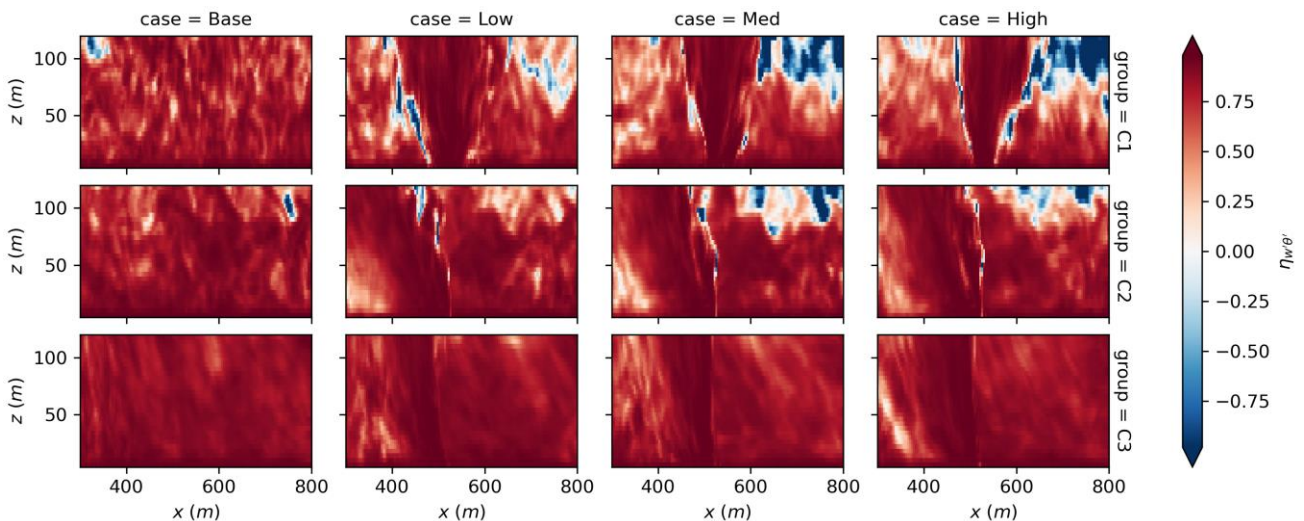

Figure 8. xz cross-section of heat transport efficiency η_{w′θ′} at the center of the domain from all cases during the first 15 minutes of the fire being set up. Each row represents different groups while each column represents either the base cases or the cases with the different fire intensities.

From both the horizontal and vertical cross-sections of the momentum transport efficiency ($\eta_{w'u'}$) (Figures 9 and 10), a new counter-gradient (negative values) momentum transport zone can also be found in the fire cases in the C1 group. This is in consistent with the analysis above and might be caused by the strong fire-induced buoyancy.
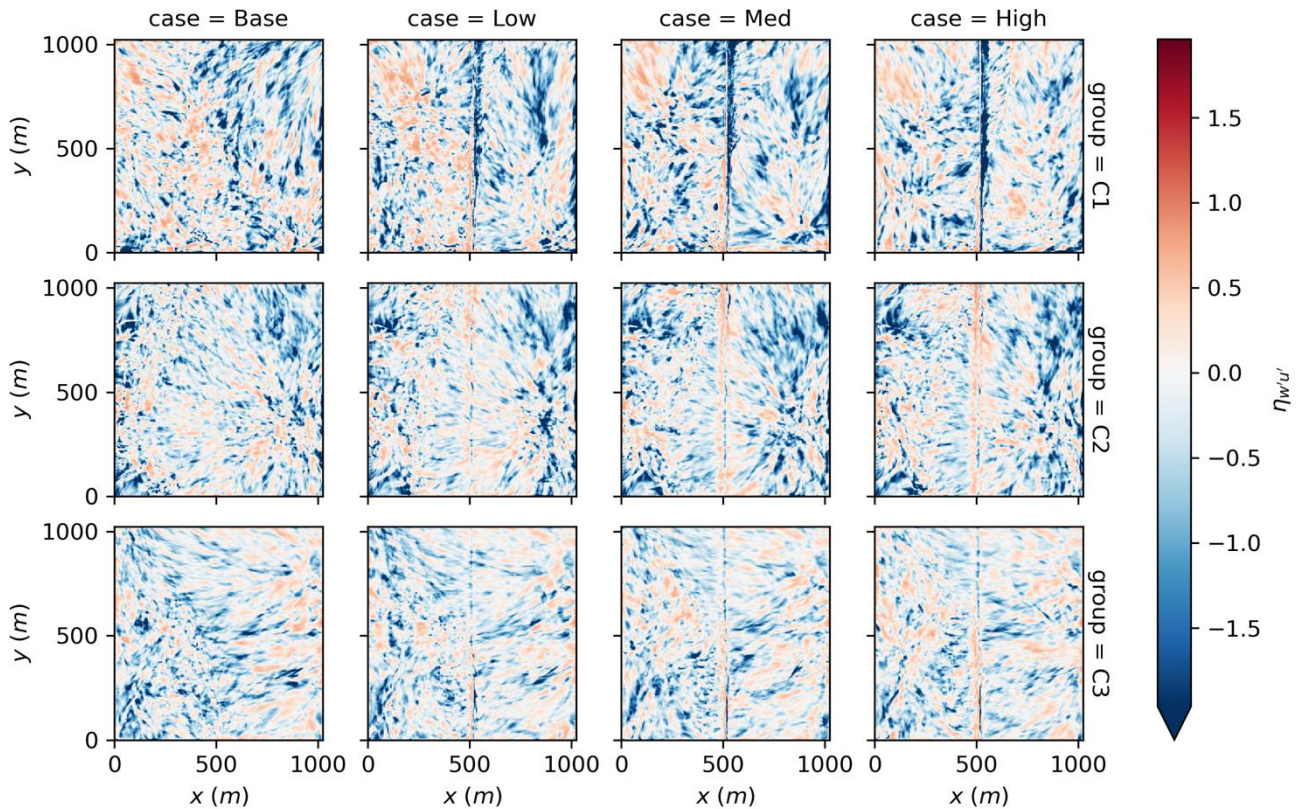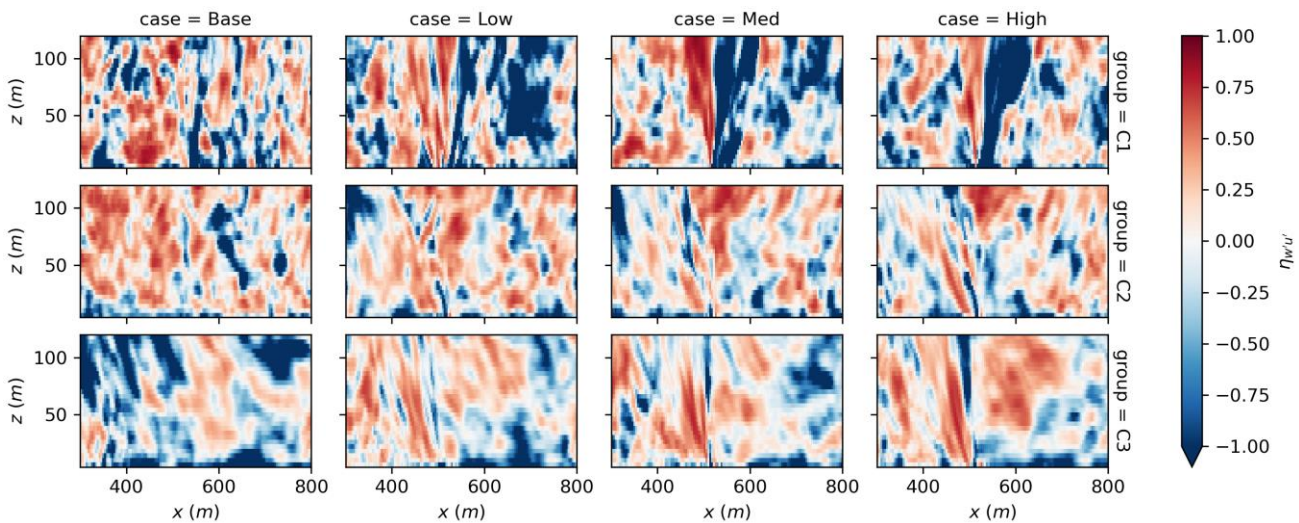
Figure 9. Horizontal cross-section of momentum transport efficiency η *at 10m above the surface from all cases during the first 15 minutes of the fire being set up. Each row represents different groups while each column represents either the base cases or the cases with the different fire intensities.*

Figure 10. xz cross-section of momentum transport efficiency η *at the center of the domain from all cases during the first 15 minutes of the fire being set up. Each row represents different groups while each column represents either the base cases or the cases with the different fire intensities.*

4. Discussion and conclusion

The study found that different convective boundary layer conditions will have different impacts in the fire-atmosphere interaction process. In a relatively weak atmospheric CBL (C1 group), our results have shown that the near-surface flow field changed substantially due to the fire-induced flow in all fire cases. The helicity analysis shows an anticorrelation between the ambient atmosphere and the fire-induced flow. The fire-induced temperature anomaly in all cases is spatially confined with a relatively narrower horizontal span compared to

other groups. The horizontal span of the anomaly is consistent with the narrow fire-induced high-efficiency heat transport zone and counter-gradient momentum transport zone. The influence of the fire-induced flow change in heat and momentum transport is extended beyond these zones to the entire near-surface region. This further suggests that fire-induced flow can be substantial in the ambient flow field and reach a large spatial extent. As a result, it would be difficult to predict fire behavior in this scenario without information about fire fuel.

On the other hand, in a stronger buoyancy driven CBL turbulence environment like the C2 and C3 groups, which represent conditions closer to typical midaltitude midday, the ambient flow field remains largely unchanged after the fire initiation. This suggests that, in an ABL with stronger buoyancy driven turbulence, the ambient atmospheric flow can play an important role in fire behavior while fire-induced flow change can be very limited. The strengthening of the vortex structures in the fire cases in the C2 group might also indicate that the ambient vortex structures could contribute to the fire whirl generation process. The fire-induced high-efficiency heat transport zone has a much wider spatial extent which is consistent with the wider extent of the temperature anomaly. The wider heat transport also leads to a weaker buoyancy flow. Unlike in the weak atmospheric CBL, there is no clear buoyancy induced counter-gradient momentum transport zone.

The results might provide guidelines to determine whether ambient atmosphere could play an important role in fire region energy transport and subsequently influence short-term fire behaviors. Future work is needed using either field campaigns or coupled fire-atmosphere models, including detailed physical and chemical processes of fire combustion and spread, to verify our results with moving fire at similar ranges of intensity.

5. Acknowledgement

6. Bibliography

Dickinson, M. B., Wold, C. E., Butler, B. W., Kremens, R. L., Jimenez, D., Sopko, P., & O'Brien, J. J. (2021). The Wildland Fire Heat Budget—Using Bi-Directional Probes to Measure Sensible Heat Flux and Energy in Surface Fires. Sensors, 21(6), 2135. https://doi.org/10.3390/s21062135

Finney, M., Cohen, J. D., Forthofer, J. M., McAllister, S. S., Gollner, M. J., Gorham, D. J., et al. (2015). Role of buoyant flame dynamics in wildfire spread. Proceedings of the National Academy of Sciences, 112(32), 9833–9838. https://doi.org/10.1073/pnas.1504498112

Kremens, R. L., Dickinson, M. B., Bova, A. S., Kremens, R. L., Dickinson, M. B., & Bova, A. S. (2012). Radiant flux density, energy density and fuel consumption in mixed-oak forest surface fires. International Journal of Wildland Fire, 21(6), 722–730. https://doi.org/10.1071/WF10143

LeMone, M. A., Grossman, R. L., Coulter, R. L., Wesley, M. L., Klazura, G. E., PouIos, G. S., et al. (2000). Land–Atmosphere Interaction Research, Early Results, and Opportunities in the Walnut River Watershed in Southeast Kansas: CASES and ABLE. Bulletin of the American Meteorological Society, 81(4), 757–780. https://doi.org/10.1175/1520-0477(2000)081<0757:LIRERA>2.3.CO;2

Li, D., & Bou-Zeid, E. (2011). Coherent Structures and the Dissimilarity of Turbulent Transport of Momentum and Scalars in the Unstable Atmospheric Surface Layer. Boundary-Layer Meteorology, 140(2), 243–262. https://doi.org/10.1007/s10546-011-9613-5

Potter, B. E. (2012). Atmospheric interactions with wildland fire behaviour - II. Plume and vortex dynamics. International Journal of Wildland Fire, 21(7), 802. https://doi.org/10.1071/WF11129

Rizza, U., Miglietta, M. M., Degrazia, G. A., Acevedo, O. C., & Marques Filho, E. P. (2013). Sunset decay of the convective turbulence with Large-Eddy Simulation under realistic conditions. Physica A: Statistical Mechanics and Its Applications, 392(19), 4481–4490. https://doi.org/10.1016/j.physa.2013.05.009

Sullivan, A. L. (2017). Inside the Inferno: Fundamental Processes of Wildland Fire Behaviour: Part 2: Heat Transfer and Interactions. Current Forestry Reports, 3(2), 150–171. https://doi.org/10.1007/s40725-017-0058-z

Wallace, J. M. (2016). Quadrant Analysis in Turbulence Research: History and Evolution. Annual Review of Fluid Mechanics, 48(1), 131–158. https://doi.org/10.1146/annurev-fluid-122414-034550

Wyngaard, J. C., & Moeng, C.-H. (1992). Parameterizing turbulent diffusion through the joint probability density. Boundary-Layer Meteorology, 60(1–2), 1–13. https://doi.org/10.1007/BF00122059

Yates, D. N., Chen, F., LeMone, M. A., Qualls, R., Oncley, S. P., Grossman, R. L., & Brandes, E. A. (2001). A Cooperative Atmosphere–Surface Exchange Study (CASES) Dataset for Analyzing and Parameterizing the Effects of Land Surface Heterogeneity on Area-Averaged Surface Heat Fluxes. Journal of Applied Meteorology, 40(5), 921–937. https://doi.org/10.1175/1520-0450(2001)040<0921:ACASES>2.0.CO;2